# Twisted Focusing of Optical Vortices with Broadband Flat Spiral Zone Plates

*Hong Liu, Muhammad Q. Mehmood, Kun Huang, Lin Ke, Huapeng Ye, Patrice Genevet, Mingsheng Zhang, Aaron Danner, Swee Ping Yeo, Cheng-Wei Qiu,\* and Jinghua Teng\**

Recent developments have shown that light's orbital angular momentum (OAM) can be harnessed for a diversity of emerging applications and generated by miniaturized OAM generators. Nanostructured flat logarithmic-spiral zone plates (LSZPs) are proposed to produce as well as focus optical vortices with a long focal depth in the broadband visible range. Topologically breaking the in-plane symmetry, this nanoengineered LSZP continuously modulates both amplitude and phase in the diffraction field to shape twisted focusing of the optical vortex beam, which is microscopically confined and spatially spiraling with variant crescent-shaped transverse intensity profiles. Owing to its rich structural degree of freedom upon aperiodic and continuously variant features, the LSZP provides a compact solution to generate and control optical vortices carrying scalable OAM and highly concentrated photons with a high transmission efficiency of ~22%. This can offer new opportunities for 3D light shaping, optical manipulation, flat optics, and photonics miniaturization and integration.

## 1. Introduction

Intensive developments have shown that light's orbital angular momentum (OAM) can be harnessed for a diversity of emerging applications,[1,2] which recently have been extended to optical communications.[3,4] From a fundamental perspective, optical vortex beams, e.g., the Lagurerre-Gaussian (LG) beam or Bessel beam, has annular transverse intensity profiles and possesses an azimuthal phase dependence of $\exp(i\ell\varphi)$ carrying a well-defined OAM of $\ell\hbar$ per photon (where $\ell$ is the topological charge indicating the winding number of helical wavefront, $\hbar$ is the reduced Planck's constant and $\varphi$ is the azimuthal coordinate).[5] Naturally OAM relates to spatial field distribution but is independent of the polarization states, which is an intriguing property to spur huge efforts to generate various optical vortices with well-developed and novel OAM generators for scrutination. For example, spatial light modulators,[3,4] holograms[6,7] and spiral phase plates[8,9] traditionally produce a typical case of LG beam, where in principle OAM can be boundlessly generated by these complex or bulky optical vortex generators. Recent achievements on plasmonic spiral vortex lens,[10,11] annular-grating vortex emitter[12] and discrete devices such as metasurfaces[13,14] as well as topological nanoslits[15] have routed research trend to downsize structure to achieve controllable OAM at a small scale. From a technological point of view, all these miniaturized devices are polarization-sensitive due to their subwavelength-scale features. In contrast, spiral zone plates (SZP) as a polarization-insensitive vortex generator has been traditionally proposed to produce integral and fractional OAM carried by either isotropic optical vortices[16,17] or anisotropic vortex beams,[18] respectively. However, it is intrinsically limited by its wavelength-dependent property. In context of light–matter interactions, spirals engineered at nanoscale, a typical class of deterministic aperiodic nanostructures, recently have stood out thanks to their structural complexity and variability in comparison with periodical matters.[19] Therefore, undertaking exploration of miniaturized novel SZP has been motivated to reach for exceptional performance.

H. Liu, L. Ke, J. Teng
Institute of Materials Research and Engineering
Agency for Science
Technology and Research (A*STAR)
3 Research Link, Singapore 117602
E-mail: jh-teng@imre.a-star.edu.sg
M. Q. Mehmood, K. Huang, H. Ye,
A. Danner, S. P. Yeo, C.-W. Qiu
Department of Electrical and Computer Engineering
National University of Singapore
4 Engineering Drive 3, Singapore 117576
E-mail: eleqc@nus.edu.sg
P. Genevet
School of Engineering and Applied Sciences
Harvard University
Cambridge, MA 02138, USA
M. Zhang
Data Storage Institute
Agency for Science
Technology and Research (A*STAR), DSI Building
5 Engineering Drive 1, Singapore 117608

## 2. Results and Discussion

Here, we propose nanostructured logarithmic-spiral zone plates (LSZP) to generate as well as focus anisotropic optical vortices with long focal depth carrying scalable OAM, which is polarization insensitive in visible range through its amplitude modulation. **Figure 1** schematically illustrates a single-armed LSZP (left-handed), a mirror image of its right-handed partner which can be mathematically interpreted in polar $(r,\varphi)$ coordinates: $r = ae^{b\varphi}$, where the radial coordinate is denoted by $r$ and
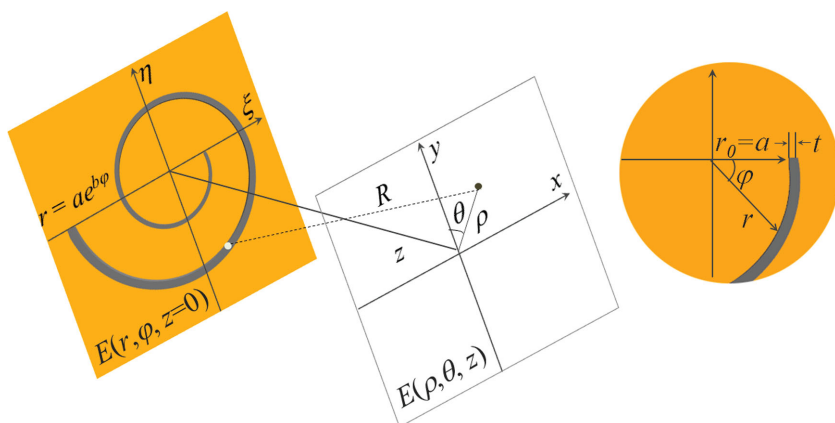
**Figure 1.** Schematic illustration of the LSZP and a cylindrical coordinate setup for the meso-field calculation to derive an analytical model. The inset shows its initial arm width $t$ = 350 nm ($\varphi$ = 0) with $3\pi$ rotation angle.

the angular coordinate by $\varphi$. The radial factor $a$ determines the initial radius whereas the azimuthal factor $b$ controls the growth rate of rotation. Together, they govern the overall structural compactness. In this case, the LSZP can be considered as a binary-amplitude mask which has negligible near-field effects upon light passing through.[20] For an incident beam of electric field $E(r,\varphi,0)$, the electric field immediately after the LSZP can be interpreted as $E(r,\varphi,0) \cdot T(r,\varphi)$, where $T(r,\varphi)$ denotes the transmission function of the structure. $\rho$ is the radial distance between a viewing point $(\rho,\theta,z)$ after the structure and the optical axis at the observation plane while $\theta$ is its azimuthal angle and $z$ is the distance between the aperture plane and the observation plane; in addition, $R$ denotes the distance between two points. To calculate the light propagation in free space, Rayleigh–Sommerfeld diffraction is applied to approximate the meso-field (within several tens of wavelengths from the structure surface).[21] For the case of multi-armed LSZP, its meso-field diffraction can be attained by coherent superposition of diffractions from individual arms. The electric field of light is given by:

$$
\begin{aligned}
&E(\rho,\theta,z) \\
&= -\frac{1}{2\pi}\sum_{m=1}^{4}\int_{0}^{3\pi}\int_{r_{m1}}^{r_{m2}} E\left(r,\varphi,0\frac{z\cdot\exp(iknR)}{R^2}\right. \\
&\left. \left(ikn-\frac{1}{R}\right)rdrd\varphi\right)
\end{aligned}
\tag{1}
$$

where $R^2 = z^2 + \rho^2 + r^2 - 2\rho r\cos(\varphi - \theta)$, $m$ is the arm number ascending from inner to outer; $r_{m1} = [(m\text{-}1)t_0 + (m\text{-}1)g_0 + a]e^{b\varphi}$ and $r_{m2} = [mt_0 + (m\text{-}1)g_0 + a]e^{b\varphi}$; $t_0$ and $g_0$ denote the arm width and separation at $\varphi$ = 0, respectively; $k$ is the wave vector of electric field and $n$ is the refractive index of the meso-regime (with $n$ = 1 in this case). Therefore, the diffraction field inclusive of spatial intensity and phase profiles of transmitted light can be acquired from Equation (1).

Unlike Bessel and LG beams, the diffractive beam in this case is a non-paraxial beam carrying OAM per photon and topological charge with different values. To reveal the vortex phase

in the diffraction field $E(\rho,\theta,z)$, the topological charge $L$ is defined as:[22]

$$
L = \frac{1}{2\pi}\oint_C d\chi
\tag{2}
$$

where $C$ refers to a closed curve (its radius is 1 um in this case) and the phase item $\chi$ = arg < $E(\rho,\theta,z)$>. For simplification and miniaturization, only the integer topological charges ($L$ = 1~4 from $P_1$ to $P_4$) will be exampled for further study. Plotted in **Figure 2**a are the diffracting fields of corresponding LSZPs. Their phase profiles explicitly show the respective integer values of topological charges, theoretically manifesting the existence of optical vortex beam produced by the LSZP. Since topological charge addressing is demonstrated merely with a single arm, the beam tends to diverge as $\ell$ rises (and even splits in half at $P_4$) based on the resulted transverse intensity profiles. It indicates that single-armed LSZP fails to effectively retain the focusing during long-range propagation.

In order to enhance the focusing performance, multiple-armed ($m$ = 4) LSZP at $P_4$ has been theoretically modeled to gain physical insight into its diffraction field by probing the correlation between the geometries of structure and transmission. Depicted in Figure 2b are the schematics of the single- and 4-armed LSZPs and their intensity profiles produced at the selected distances ($z$ = 6.25 μm, 15 μm, and 21 μm). With the same structural factors ($a,b,t$), the 4-armed spiral exhibits much superior focusing ability to its single-armed opponent in terms of photon confinement along long-range propagation. It validates that more arms strengthen the constructive interference to enhance focusing performance of the LSZP, which is similar to Fresnel lens and zone plates.

Upon a normal incident illumination ($\lambda$ = 632.8 nm) from the backside, the spatial intensity distributions of the 4-armed LSZP are analytically plotted in **Figure 3**. Centered on the optical axis, oblique transmission rays are visualized along the $x$–$z$ plane as shown in Figure 3a. In contrast, zero intensity (dark center) has been attained along the beam-axis. To further demonstrate the spatial intensity distribution, a summary of pseudo-color intensity maps over selected $x$–$y$ transverse planes at different heights along the propagation direction ($z$) are depicted in Figure 3b. As diffracted light propagates, foci of crescent transverse profiles are anisotropically formed as well as confined in a microscopic circular area of a diameter less than $\approx$3 μm from the initialization at z $\approx$ 4 μm ($\approx$6.3$\lambda$) till a distance of about 32 μm, beyond which a continual decay of photon density and gradually decreased confinement of transverse intensity profile are observed. A relatively long depth of focus approximates 44$\lambda$ along which the transverse radii of foci gradually rise with a common feature of dark center. Up to this point, an interesting scenario intuitively comes about where the LSZP produces and focuses an optical beam with left-handed twisting around its beam-center in a conical trajectory when travelling in free space.

www.MaterialsViews.com

ADVANCED
OPTICAL
MATERIALS
www.advopticalmat.de

FULL PAPER
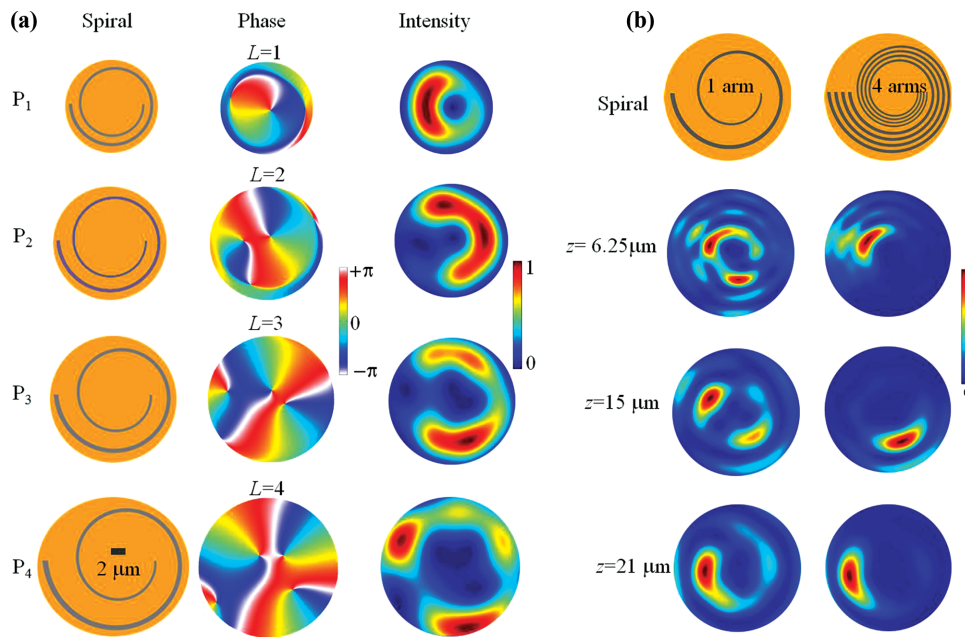
**Figure 2.** Scaling of topological charge carried by the optical beam. (a) A summary of different LSZPs constructed by the scaling factors of four examples and their corresponding phase and intensity profiles ($z = 10$ μm). The scaling factors were exampled as follows: $P_1$ ($a = 4.2$ μm, $b = 0.04$); $P_2$ ($a = 4.31$ μm, $b = 0.053$); $P_3$ ($a = 4.45$ μm, $b = 0.07$); $P_4$ ($a = 4.59$ μm, $b = 0.0875$). (b) FDTD analysis and comparison of arm number effect on focusing performance at the meso-field between the single- and 4-armed LSZP structures ($P_4$).

The spatial intensity distribution is explicitly visualized by the FDTD-generated three-dimensional normalized maximum intensity $|E_{max}|^2$ depicted in **Figure 4**a. It shows the generated beam continuously twists around its beam-axis and alters its intensity during propagation. Its projection onto the transverse plane describes a logarithmic-spiral path, indicating that actually a spiraling optical beam is shaped due to the twisted

focusing of the LSZP. Figure 4b plots the computed Poynting vector $S$ corresponding to the maximum intensity, showing that the resultant Poynting vectors are directed tangentially compelling a conically spiraling energy flow around the beam axis, which is due to the contributions from the azimuthal component $S_\theta$ and the longitudinal component $S_z$. Hence, the produced beam theoretically satisfies the fundamental criteria of
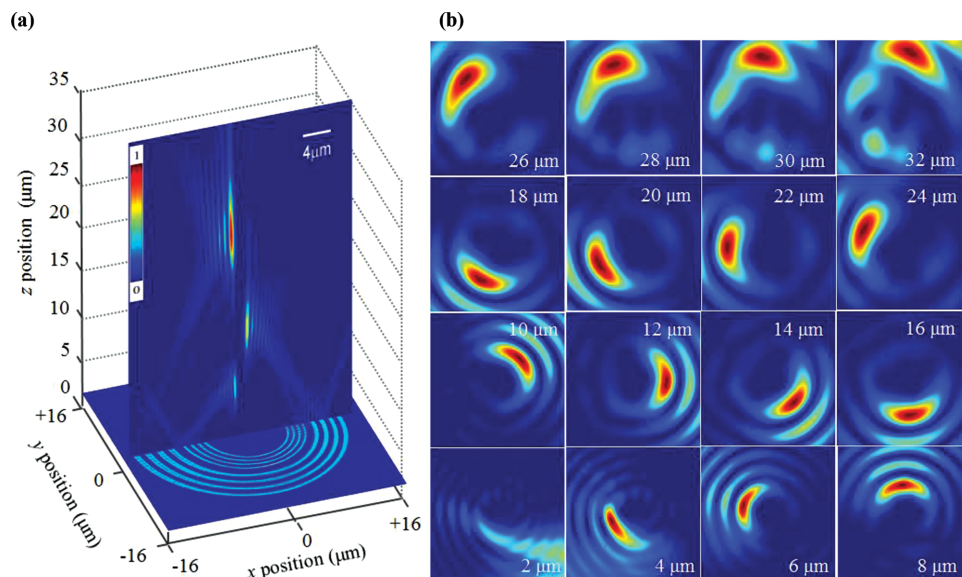


**Figure 3.** The analytical pseudo-color intensity maps of spatial transmission along the optical axis above the 4-armed LSZP structure. The initial separation ($g_0$) between the arms is 350 nm (equal to $t_0$). (a) The intensity profiles of $x$–$z$ plane across the spiral center ($16 \times 35$ μm$^2$). The bottom panel shows the intensity image ($16 \times 16$ μm$^2$) at the surface ($z = 0$). (b) A summary of the $x$–$y$ plane intensity profiles over an area of $4 \times 4$ μm$^2$ at selected heights. The color scale in each image is normalized to its respective maximum intensity in order to facilitate distinct visualization.
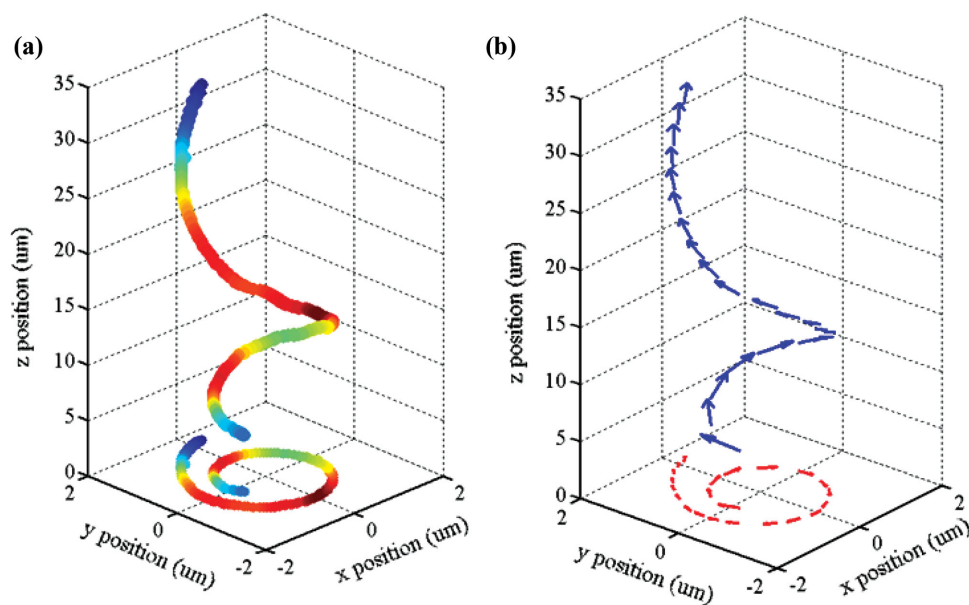
**Figure 4.** FDTD analysis of spatial profile of the maximum intensity $|E_{max}|^2$ and the corresponding transmitted energy flux (Poynting vector). (a) Numerically calculated three-dimensional ($xyz$) spatial profile of $|E_{max}|^2$ above the structure surface. The bottom panel shows its projection onto the $xy$ plane. The color scale is normalized to its respective maximum intensity. (b) Numerically calculated Poynting vectors of the diffracted optical beam are directed along a conical trajectory. Its projection onto the $xy$ plane showing the transverse part ($x$ & $y$ components) is depicted in the bottom panel.

an OAM-carried vortex beam, which is signified by its central dark region and spiraling $S$ around its axis.[23]

**Figure 5**a schematically depicts the optical characterization using a photon scanning tunneling microscope (PSTM: Alpha 300S, WITec GmbH) illuminated by a linearly polarized (LP) continuous wave He-Ne laser. The scanning electron microscopy (SEM) image (the inset) shows the LSZP specimen embedded in a 100-nm thick chromium film on a quartz substrate via electron beam lithography. A summary of the measured pseudo-color intensity maps depicted in Figures 5b & 5c demonstrate good agreement with the theoretical descriptions. Based on the above studies, the origin of focusing cum twisting can be qualitatively elaborated as following. Upon illumination, light passing through the spiral will be imposed by the geometrical phase of each individual arm. The optical path length of each diffractive beam is uniquely modulated by the variant geometry of the LSZP leading to phase aberration. Such phase aberration accumulates along propagation, which is eventually accountable for exponential-angular-dependent constructive interference to consecutively form twisted focusing as well as vary intensity in free space. Simultaneously, the propagation vectors $\left(\vec{k}\right)$ of diffracted beams spatially superimpose at corresponding locations, which governs the twisting of the beam around the $z$-axis following a conical trajectory. Hence, the focusing-cum-twisting phenomenon can be qualitatively attributed to the in-plane symmetry breaking intrinsically determined by the logarithmic-spiral algorithm. A detailed analysis given in the Supporting Information (SI) shows that this phenomenon is wavelength-dependent due to the broadband behavior of the device. Note this LSZP exponentially grows its features (widths and separations) with the angle over a scale from sub- ($\approx0.55\lambda$) to slightly above one-wavelength ($\approx1.27\lambda$). Within such a scale, the subwavelength control of wavefronts

via metasurfaces has been demonstrated in a rather broad range of wavelength upon acquiring new degree of freedom.[24] Therefore, it is understandable that this LSZP is also operateable under broadband illumination from a supercontinuum laser source (Fianium, FemtoPower 1060, wavelength ranges approximately from 420 nm~2 μm), as shown in the Supplementary Movies.

To measure the phase profile, a Mach-Zehnder interferometer was set up to interfer the spiraling beam with a co-propagating Gaussian beam. **Figure 6**a presents the FDTD-generated results for the helical phase profile of optical vortex beam with the topological charge of $L = +4$ and phase shift ranging from 0 to $8\pi$ (with an incremental step of $2\pi$). Under spherical wave interference, spiral wavefront of this vortex beam was manifested by four anti-clockwise twisted fringes as shown in Figure 6b, indicating a topological charge of $L = +4$. The simulated intensity distribution of the interference pattern with a close-up visualization at the interference center completely reconstructs the spiral optical wavefronts as shown in Figure 6c. Intensity discrepancy of those 4 spiral fringes between Figures 6b and 6c can be observed. It can be attributed to the limited degree of coherence of light source and narrow tuning range of the optical path for both the sample and reference beams due to the optical setup with the PSTM system, which makes it very challenging to achieve a perfectly matched experimental image.

In addition, polarization dependence of twisted focusing via this LSZP was also scrutinized under LP, left- & right-handed circularly polarized (LHCP and RHCP) incidences, respectively. **Figure 7** shows the FDTD results, which is in good agreement with experimental results. Under either LHCP or RHCP incidences, the transmission always exhibits the same polarization state; i.e., LHCP incidence yields LHCP
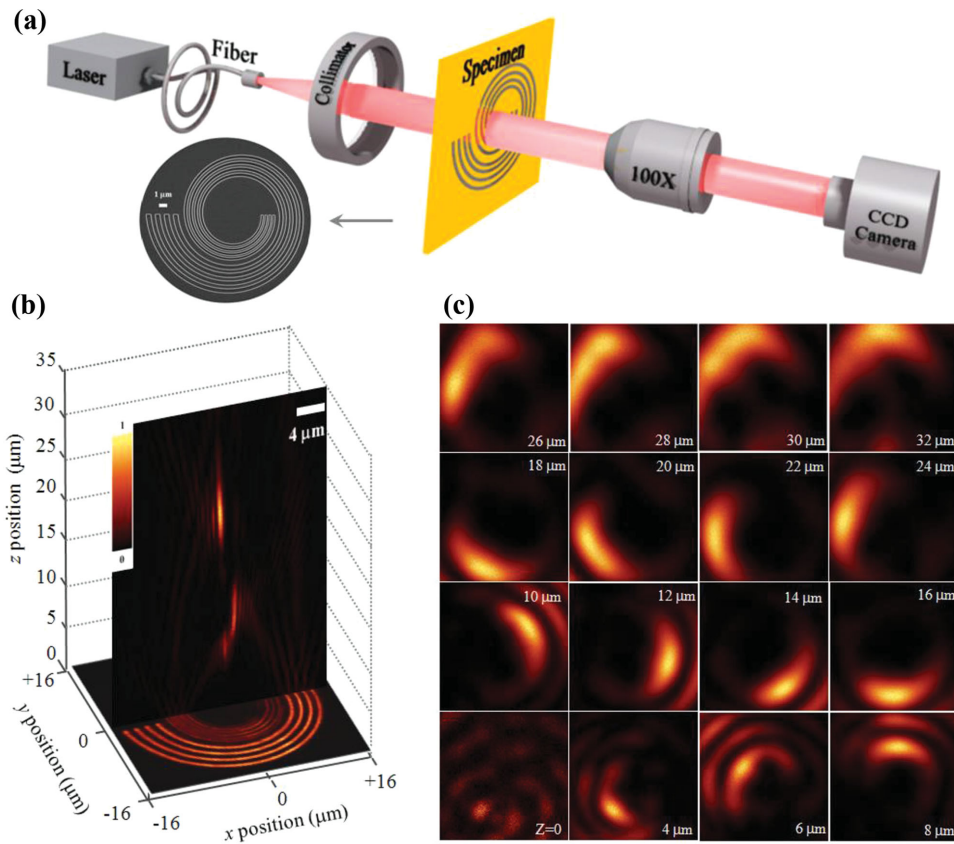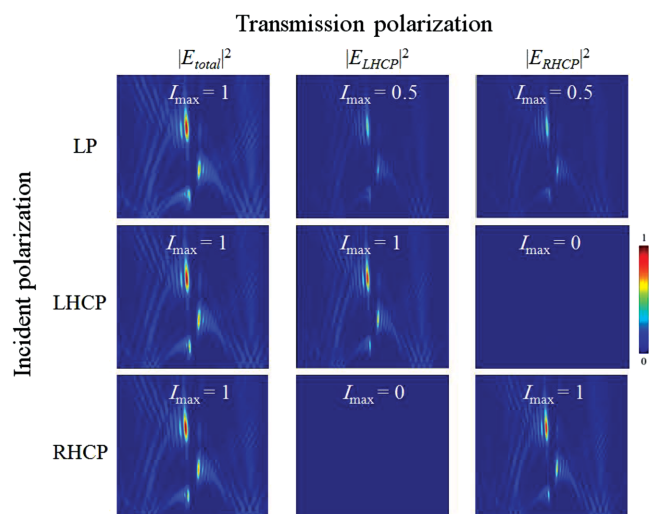
**Figure 5.** Characterization of the twisted focusing of optical vortex beam produced by the 4-armed LSZP. (a) Experimental setup and the SEM image of the fabricated specimen (the inset). (b) The intensity mapping of x–z plane measured across the spiral center via a depth scan ($16 \times 35$ μm$^2$). The inset (bottom panel) shows the intensity image ($16 \times 16$ μm$^2$) at the surface, which is taken at the image plane of the objective lens ($z = 0$). (c) A summary of the x–y plane intensity maps measured over an area of $3 \times 3$ μm$^2$ at selected heights above the surface. The color scale in each image is normalized to its respective maximum intensity in order to facilitate distinct visualization.

transmission while RHCP incidence produces RHCP transmission with equal intensities measured in both cases. In contrast, under LP incidence, the transmitted beam simultaneously comprises LHCP and RHCP beams with intensities equal to the half of $|E_{total}|^2$. It can be explained that this LSZP varies its arm width from subwavelength (inner) to above-one-wavelength scale (outer). The transmission from subwavelength features is polarization sensitive, which has been well verified by quite a few reported studies. However, in this case,

the transmitted beam from the features of above-one-wavelength scale is insensitive to polarization states, which dominates the diffraction field. Therefore, the overall transmission of this LSZP exhibits polarization-insensitivity, which is dominated by the diffraction from large feature (above-wavelength scale) over than that from small feature (sub-wavelength scale). A high transmission efficiency of about 22% has been experimentally measured, which is identical to the analytical result as detailed in the SI.
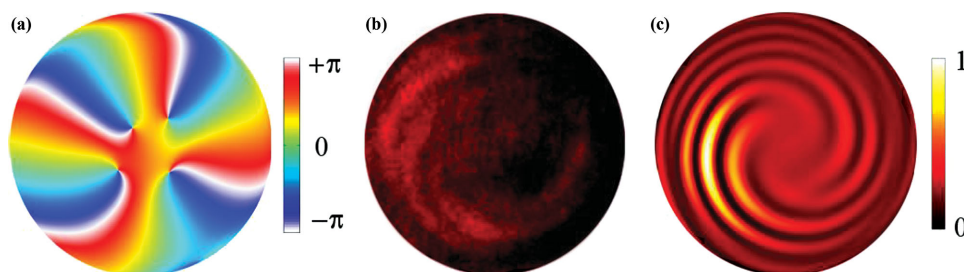


**Figure 6.** Computational and experimental phase profiles reveal by interference. (a) FDTD-produced helical phase profile at the center of the optical vortex beam in a circular area of 3-μm diameter with a topological charge $L = +4$. (b) Measured 4-spiral pattern with a topological charge $L = +4$. In contrast to the bright fringes, the core region exhibits a much lower intensity and becomes undetectable by the CCD camera. (c) FDTD-produced 4-spiral pattern under spherical wave interference at the center of a circular area with a diameter of about 4 μm, which is well reconstructed with reference to experiment.

ADVANCED
OPTICAL
MATERIALS

www.advopticalmat.de

Materials Views
www.MaterialsViews.com

FULL PAPER

**Transmission polarization**



**Figure 7.** FDTD-produced results of incident polarization vs transmission polarization. Numerically calculated spatial intensity mapping of the $xz$ plane across the spiral center is collected over an area of $16 \times 35$ μm$^2$. In each row under LP, LHCP and RHCP incidences, the color scale of images is normalized to the maximum of total field intensity $|E_{total}|^2$ as depicted in the leftmost images, respectively. The normalized intensities are indicated on top of the calculated intensity maps.

## 3. Conclusions

To summarize, in combination with the theoretical modeling, numerical simulation and experimental verifications, it rigorously affirms that the LSZP is able to shape twisted focusing of polarization-insensitive optical vortex beam to be microscopically confined during propagation with a long depth of focus with high transmission efficiency. The diffracted beam spatially propagates with variant transverse intensity profiles in contrast to traditional spiralling waves of invariant profiles.[25] Owing to its intrinsically rich degree of freedom to govern the interaction with light, the nanostructured LSZP is able to produce controllable and scalable OAM with broadband behavior, which can be realized for every region of the optical spectrum. The LSZP can potentially act as an inexhaustible-OAM turbine and opens up a new avenue for manipulating light's OAM at higher photon density, which will find applications from quantum OAM processing to 3D light shaping for transportation and rotation of small particles in optical tweezers as well as laser processing of complex structures and flat optics. The same type of spiral structures could be engineered to twist and focus other waves such as acoustic waves or even matter waves.

## Acknowledgements

[1] M. Yao, M. J. Padgett, *Adv. Opt. Photon.* **2011**, *3*, 161.
[2] M. J. Padgett, R. Bowman, *Nature Photon.* **2011**, *5*, 343.
[3] J. Wang, J.-Y. Yang, I. M. Fazal, N. Ahmed, Y. Yan, H. Huang, Y. Ren, Y. Yue, S. Dolinar, M. Tur, A. E. Willner, *Nature Photon.* **2012**, *6*, 488.
[4] N. Bozinovic, Y. Yue, Y. Ren, M. Tur, P. Kristensen, H. Huang, A. E. Willner, S. Samachandran, *Science* **2013**, *340*, 1545.
[5] L. Allen, M. W. Beijersbergen, R. J. C. Spreeuw, J. P. Woerdman, *Phys. Rev. A* **1992**, *45*, 8185.
[6] V. Yu. Bazhennov, M. V. Vasnetsov, M. S. Soskin, *JETP Lett.* **1990**, *52*, 429.
[7] Y. Ren, M. Li, K. Huang, J. Wu, H. Gao, Z. Wang, Y. Li, *Appl. Opt.* **2010**, *49*, 1838.
[8] M. W. Beijersbergen, R. P. C. Coerwinkel, M. Kristensen, J. P. Woerdman, *Opt. Commun.* **1994**, *112*, 321.
[9] G. A. Turnbull, D. A. Robertson, G. M. Smith, L. Allen, M. J. Padgett, *Opt. Commun.* **1996**, *127*, 183.
[10] Y. Gorodetski, A. Niv, V. Kleiner, E. Hasman, *Phys. Rev. Lett.* **2008**, *101*, 043903.
[11] Y. Gorodetski, A. Drezel, C. Genet, T. W. Ebbesen, *Phys. Rev. Lett.* **2013**, *110*, 203906.
[12] X. Cai, J. Wang, M. J. Strain, B. Johnson-Morris, J. Zhu, M. Sorel, J. L. O'Brien, M. G. Thompson, S. Yu, *Science* **2012**, *338*, 363.
[13] N. Yu, P. Genevet, M. A. Kats, F. Aieta, J.-P. Tetienne, F. Capasso, Z. Gaburro, *Science* **2011**, *334*, 333.
[14] P. Genevet, N. Yu, F. Aieta, J. Lin, M. A. Kats, R. Blanchard, M. O. Scully, Z. Gaburro, F. Capasso, *Appl. Phys. Lett.* **2012**, *100*, 013101.
[15] E. Brasselet, G. Gervinskas, G. Seniutinas, S. Juodkazis, *Phys. Rev. Lett.* **2013**, *111*, 193901.
[16] N. R. Heckenberg, R. McDuff, C. P. Smith, A. G. White, *Opt. Lett.* **1992**, *17*, 221.
[17] Z. Jaroszewicz, A. Kolodziejczyk, *Opt. Commun.* **1993**, *102*, 391.
[18] L. Wei, Y. Cao, X. Wen, Z. Zhao, L. Cao, Y. Gu, *J. Opt. Soc. Am. A* **2013**, *30*, 233.
[19] L. D. Negro, S. V. Boriskina, *Laser Photon. Rev.* **2012**, *6*, 178.
[20] G. Rui, R. L. Nelson, Q. Zhan, *Opt. Express* **2012**, *20*, 18819.
[21] D. C. O'Shea, T. J. Suleski, A. D. Kathman, D. W. Prather, *Diffractive Optics: Design, Fabrication, and Test*, Ch. 2, SPIE Press, Washington, USA **2004**.
[22] M. R. Dennis, *Opt. Commun.* **2002**, *213*, 201.
[23] M. J. Padgett, J. Courtial, L. Allen, *Physics Today* **2004**, *57*, 35.
[24] X. Ni, N. K. Emani, A. V. Kildishev, A. Boltasseva, V. M. Shalaev, *Science* **2012**, *335*, 427.
[25] C. A. Alonzo, P. J. Rodrigo, J. Glückstad, *Opt. Express* **2005**, *13*, 1749.